Journal of Alloys and Compounds 718 (2017) 236–245

Contents lists available at ScienceDirect

Journal of Alloys and Compounds

journal homepage: http://www.elsevier.com/locate/jalcom

Bandgap engineering of $Cu_2ZnSn_{1-x}Ge_xS(e)_4$ by adjusting Sn-Ge ratios for almost full solar spectrum absorption

Guilin Chen [a, c, *, 1], Weihuang Wang [a, 1], Shuiyuan Chen [a], Zhezhe Whang [a], Zhigao Huang [a, c], Biyun Zhang [a], Xiangkai Kong [b, **]

[a] Fujian Provincial Key Laboratory of Quantum Manipulation and New Energy Materials, College of Physics and Energy, Fujian Normal University, Fuzhou, 350007, China
[b] School of Physics and Electronic Information, Huaibei Normal University, Huaibei, Anhui, 235000, China
[c] Fujian Provincial Collaborative Innovation Center for Optoelectronic Semiconductors and Efficient Devices, Xiamen, 361005, China

ARTICLE INFO

Article history:
Received 14 February 2017
Received in revised form
8 May 2017
Accepted 14 May 2017
Available online 15 May 2017

Keywords:
$Cu_2ZnSn_{1-x}Ge_xS(e)_4$
Thin films
Band gap engineer
Germanium

ABSTRACT

The substitution of Sn with Ge is one of the promising approaches to fabricate high-efficiency $Cu_2ZnSn_{1-x}Ge_xS(e)_4$ (CZTGS(e)) thin-film solar cells, especially for the multijunction or bandgap-graded solar cells. However the evolution of structure and optical properties of CZTGS(e) in a wide composition range ($0 \leq x \leq 1$) hasn't been researched and elucidated systematically. In this paper, CZTGS(e) films were synthesized by selenizing or sulphidising oxide precursors, and their optical, componential and structural property were investigated by absorption spectroscopy, scanning electron microscopy and X-ray diffraction (XRD)/Raman, respectively. The insertion of germanium into the lattice of $Cu_2ZnSnS(e)_4$ (CZTS(e)) is verified by relevant XRD peaks and Raman vibrational modes, as both of them shift towards higher diffraction angles and wave-numbers respectively. Besides, the spectrum of absorption revealed that the bandgap of CZTGS(e) can be widely adjusted between 0.96 and 2.0 eV. The preliminary solar cells show that the Voc increases with the increase of bandgap, while the Jsc exhibits opposite tendency. This can be expected to be applied in full solar spectrum absorption.

1. Introduction

Recently, $Cu_2ZnSn_{1-x}Ge_xS(e)_4$ (CZTGS(e)) thin films have drawn great attention as an absorber materials for solar cells, due to the earth-abundant and low-cost constituent materials [1]. A champion efficiency (up to 12.6%) device has been created by using $Cu_2ZnSn(S_xSe_{1-x})_4$ (CZTSSe) absorber material [2]. However, it is still far from the 22.6% achieved for $Cu(In,Ga)Se_2$ (CIGSe) solar cells, lets alone the maximum efficiency (31%) limited by the theory of Shockley and Queisser [3,4]. The CIGSSe thin films with gradient bandgap are mainly engineered by changing S/Se or Ga/In ratios, which has been proven as an important way to improve the performance of CIGSSe solar cells [5,6]. Similarly, the bandgap of CZTGS(e)-based thin films grading can possibly be achieved by two ways, as seen in Fig. 1. First, through adjusting the S/Se ratio, the $Cu_2ZnSn(S_xSe_{1-x})_4$ (CZTSSe) and $Cu_2ZnGe(S_xSe_{1-x})_4$ (CZGSSe) thin films have an adjustable direct bandgap with range of (1.0–1.5 eV) and (1.5–2.0 eV), respectively [7–10]. However, taking control of the bandgap value precisely via adjusting the S/Se ratio is challenging, due to the high volatility of elements (S and Se). Another promising strategy for tailoring the band gap is partial substitution of tin (Sn) with germanium (Ge) in the CZTS(e) lattice, which is the same principle as using gallium (Ga) to take the place of indium (In) in CIGSSe. Similarly, element Sn can be replaced by an isoelectronic and lower atomic number element (Ge). It will tune the band gap primarily through modification of the IV-VI sp-orbital anti-bonding of the conduction band edge. For example, the bandgap of CZTGSe and CZTGS films can be tuned feasibly with range of (1.0–1.5 eV) and (1.5–2.0 eV) through changing Sn/Ge ratio, which can avoid the rough control of the S/Se ratio during annealing [11–13]. In addition to band gap tuning, CZTGS(e) has also been suggested to modify the formation of unfavorable defects, because Ge^{IV+} also has the benefit

* Corresponding author. Fujian Provincial Key Laboratory of Quantum Manipulation and New Energy Materials, College of Physics and Energy, Fujian Normal University, Fuzhou, 350007, China.
** Corresponding author.
E-mail addresses: glchen@fjnu.edu.cn (G. Chen), kxk@chnu.edu.cn (X. Kong).
[1] These authors contributed equally to this work and should be considered co-first authors.

http://dx.doi.org/10.1016/j.jallcom.2017.05.150
0925-8388/

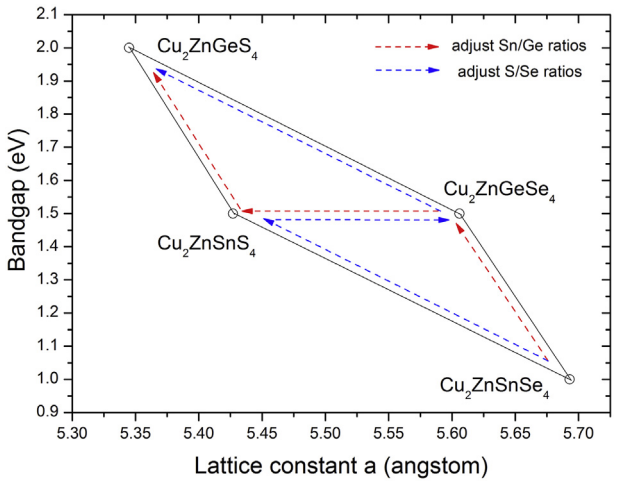

Fig. 1. Schematic diagram for engineering the band gap of CZTGS(e) thin films by adjusting Sn/Ge or S/Se ratios.

of being less likely than Sn^{IV+} to bring a transformation in oxidation state when the device operates [11,14].

To date, many researchers have reported the engineering of the band gap of CZTGS(e) thin films by adjusting Sn/Ge ratios [15,16]. However, most of them only tune the band gap in a narrow range (0.5eV), e.g. 1.0eV (CZTSe) ~ 1.5eV (CZGSe), 1.5eV (CZTS) ~ 2.0eV (CZGS), as well as fixed value. For instance, Grossberg et al. [16] have observed a continuous change from 0.955 eV to 1.364 eV of the PL in CZTGSe compounds with various Ge/Sn ratios. Both Mitzi et al. [11], Kim et al. [17], Neuschitzer et al. [18] and Khadka et al. [19] have presented the enhancement of CZTGSSe devices performance by using fixed Ge content absorber. Kim et al. [12] have synthesized bandgap-graded CZTGS thin films by varying the Ge content. However, the reported data on wide range (1.0–2.0eV) tuning of band gap through Ge/Sn ratios in CZTGS(e) films are quite meager. Khadka et al. [20] have prepared CZTGS(e) thin films through the spray-based deposition method. The band gap energy of postsulfurized CZTGS thin films and postselenized CZTGSe thin films shows 1.51–1.91eV and 1.07–1.44eV, respectively. But there is still lacking systematic studies on preparation and properties of CZTGS(e) thin film with wide tunable band gap (different Ge/Sn ratios) using other method, which are expected to improve the performance of device effectively.

In this work, the CZTGS(e) thin films were synthesized by selenizing or sulphidising oxide precursors. The oxide nanoparticles were first employed in these Ge-substituted CZTGS(e) thin films, as it has a great degree control of the ingredient ratio of the final thin films. In addition, the oxides (e.g. GeO_2) are stable either in air or moisture condition, which can avoid using the typical hazardous, moisture sensitive germanium precursor (e.g.$GeCl_4$) and expensive sputtered Ge metal layers [21–23]. The effects of Ge on the compositional, structural and optical properties of CZTGS(e) thin films were revealed. The preliminary CZTSe, CZTS and CZGS devices with different bandgap show efficiency of 3.4%, 3.08% and 0.7% respectively. The effects of bandgap on the Voc and Jsc were also discussed, which are expected to use in high efficient graded-bandgap single-junction or multi-junction solar cell in the further studies.

2. Experimental

First of all, the required mass of metal salts were mixed and grounded with excess ammonium bicarbonate (0.1mol) until to form uniform distributions of metal elements. Then the mixture was baked at 380 °C for about an hour to get oxide powders. The metal salts were 0.01 mol $Zn(NO_3)_2 \cdot 6H_2O$, (0.01-x) mol SnC_2O_4, x mol GeO_2 and 0.02 mol $Cu(NO_3)_2 \cdot 3H_2O$ (Cu/Zn/Sn/Ge ratio = 2/1/(1–100x)/100x), where Ge content is x = 0, 0.0025, 0.005, 0.0075, 0.01 mol. After that, the mixing oxide nanoparticles were dispersed in ethanol, forming a uniform oxides ink. The ink contained germanium dioxide used in this work is nontoxic and air & moisture stable, which is stored for several months. Secondly, the oxides were coated on the soda lime glass substrates with doctor blade process. Finally, the oxides films were sulfurized at 550 °C for 30min under vacuum condition (base ~10^{-1}Pa) and adopted solid S as the source of S vapor. To prepare CZTGSe thin films, the sulfurized CZTGS thin films were sequentially selenized with Se vapor under flowing Ar. The selenization temperature was fixed at 580 °C for 30 min, keeping the heating rate fixed at 50 K/min. To reach the target temperature, the samples will go through low temperature annealing within 11 min.

After the CZTGS(e) thin films were deposited on molybdenum coated glass substrate, photovoltaic devices were completed by the chemical bath deposition of CdS, sputtering of i-ZnO (50 nm), ZnO:Al (400 nm) and silver paint as the top electrode. The CZTGS(e) thin film composition for the cell performance measurement were fixed at approximately Cu/(Zn + Sn + Ge) = 0.8 and Zn/(Sn + Ge) = 1.2.

The XRD method (D/Max-rA) was used to identify the lattice structure of the CZTGS(e) films. A field emission scanning electron microscope (FESEM, JEOL-JSM-6700F) was applied to observe the morphology of the CZTGS(e) films. A spectrophotometer was used for recording the optical absorption spectrum of the CZTGS(e) films. The chemical composition of the CZTGS(e) films was identified by EDX (Energy Dispersive X-Ray Spectroscopy, energy 20 keV). The Raman spectra of the CZTGS(e) films were measured at room temperature via a LABRAM-HR micro-Raman system with a laser source of 514 nm. The performances of the devices were tested under standard AM1.5 conditions (100 mW/cm^2; 25 °C). The external quantum efficiency (EQE) of devices was characterized using an incident PCE measurement unit (PV measurement, Inc., USA).

3. Results and discussions

Table 1 shows the elemental composition obtained from EDX for oxide precursors thin films, sulfurized CZTGS thin films and selenized CZTGSe thin films with different Ge content. Accounting that the measured values of EDX contain ±5% errors, for all films, the Cu: Zn: Sn: Ge ratio is no less than the proportion of the initial materials, the quantity of the constituent elements remains nearly the same even after powder synthesis and annealing process. Therefore, the oxides-based route is considered as one of facile process for CZTGS(e) thin films with controllable composition.

For the annealed thin films, it can be observed that there is a similar step of Ge/Sn ratio (Ge replace Sn) in both CZTGS and CZTGSe thin films when the initial composition of $Cu_2ZnSn_{1-x}Ge_xO_y$ varies x from 0 to 1 with a step of 0.25, as presented in Table 1. From the literature, it is easy to take place a significant loss of Sn or Ge in the annealing (sulfurization or selenization) process because the Sn sulfides/selenides (SnS/SnSe) or Ge sulfides/selenides (GeS/GeSe) will form high pressure vapor at high processing temperature [24,25]. In our previous work, the loss of tin was alleviated during the synthesis of CZTS thin films, which was attributed to the stability of oxides [26]. The control of Sn plays an important role in the preparation of CZTS material for solar cell. During the high temperature annealing steps, Sn not only exists in solid state CZTS films but also gas state SnS. The high volatility of SnS makes it hard to

Table 1
Element composition of oxides precursor thin film, CZTGS thin films and CZTGSe thin films with different Ge content measured by EDX.

Raw materials	Cu (at%)	Zn (at%)	Sn (at%)	Ge (at%)	O(at%)	S (at%)	Se (at%)
$CZTO_X$	16.88	8.37	8.50	–	66.24	–	–
$CZT_{0.75}G_{0.25}O_x$	17.70	9.15	6.67	2.17	64.31	–	–
$CZT_{0.5}G_{0.5}O_x$	18.83	9.58	4.52	4.51	62.56	–	–
$CZT_{0.25}G_{0.75}O_x$	18.44	9.63	2.35	7.03	62.56	–	–
$CZGO_x$	20.97	10.22	–	10.96	57.85	–	–
$CZTS_4$	25.52	12.43	12.75	–	–	49.31	–
$CZT_{0.75}G_{0.25}S_4$	25.21	12.90	9.43	3.25	–	49.22	–
$CZT_{0.5}G_{0.5}S_4$	24.81	12.58	6.25	6.80	–	49.58	–
$CZT_{0.25}G_{0.75}S_4$	25.07	11.82	2.94	11.42	–	48.75	–
$CZGS_4$	25.30	12.03	–	12.76	–	49.91	–
$CZTSe_4$	26.68	12.74	12.35	–	–	2.62	45.61
$CZT_{0.75}G_{0.25}Se_4$	26.59	12.69	9.80	2.60	–	2.57	45.75
$CZT_{0.5}G_{0.5}Se_4$	24.96	13.50	6.70	5.79	–	2.53	46.51
$CZT_{0.25}G_{0.75}Se_4$	25.22	12.95	3.30	9.48	–	2.61	46.45
$CZGSe_4$	25.34	13.64	–	11.72	–	1.96	47.33

precisely control Sn. Once the SnS losses from the solid thin films, it will lead to ZnS and CuS secondary phases in the CZTS thin films. So the controllable Sn losses are critical for CZTS growth. Here, we proposed a model for our oxides routes to explain the role of Sn in CZTS growth, as shown in Fig. 2. The stability of SnO_2 is relative higher than that of CuO and ZnO. At the low sulfurization temperature, CuO and ZnO were preferentially converted into CuS and ZnS respectively (Fig. 2(b)). As the temperature increases to high temperature, the SnO_2 begin to convert into SnS_2 (Fig. 2(c)). The resulted SnS_2 was immediately surrounded and reacted with the abundant CuS and ZnS, forming CZTS phase. Therefore, the losses of Sn can be eliminated using such an oxides route. Fortunately, such a great degree of composition (especially Sn and Ge) control was also observed in the Ge-alloyed CZTGS or CZTGSe thin films in this work.

It is also noted that no oxygen content is detectable within the limit of EDX analysis, indicating that the oxides were completely converted into sulfides or selenium after the sulfurization or selenization process. A comprehensive analysis was tested by using XPS (X-ray photoelectron spectroscopy) in our previous [26], which also provided a support to affirm the absence of oxygen in the annealed films. From the perspective of bond energy, oxygen seems to be hard to convert into sulfides or selenium under equilibrium state. Because the bond dissociation energy of Ge-O (~657.5 kJ/mol) is higher than those of Ge-S (~534 kJ/mol) and Ge-Se (~484.7 kJ/mol). Also, Sn related bonds show similar tendency. However, the films were suffered from non-equilibrium condition during sulfurization or selenization in this work. The films were annealed at high temperature under S or Se vapor. One side, the high temperature will provide sufficient energy for the reaction. On the other hand, the vapor pressure will rise as the increase of temperature in the close reactor. The ultra-high vapor pressure make the reaction is in the non-equilibrium state. This will promote the reaction. When the sulfurization or selenization were completed, the sulfur content in the sulfurized CZTGS thin films were 48.75–49.91 at% ([S]/metals were 95–99%). However, after the selenization of CZTGS thin films, the sulfur content was rapidly decreased to 1.96–2.62 at%, while selenium content was significantly increased to 45.61–47.33 at% ([Se + S]/metals were 93–97%). Both [S]/metal and [Se + S]/metals are slightly lower than ideal value (100%), indicating the formation of S or Se vacancy. This can be explained by the fact that when sulfur or selenium pressure is low during the cooling process, some of the lattice sulfur or selenium may be released in the form of sulfur or selenium vapor, thus leaving sulfur or selenium vacancies. It should be noted that sulfur was nearly replaced by selenium during selenization of CZTGS, and only minor concentrations of S left in the crystal lattice. So "CZTGSe' was used for the selenized sample throughout this paper. Therefore, such an oxides-based route can be used to prepare pure CZTGS(e) thin films and keep the metal elements in the control after the high temperature annealing.

The XRD patterns of the $Cu_2Zn(Sn_{1-x}Ge_x)Se_4$ and $Cu_2Zn(Sn_{1-x}Ge_x)S_4$ thin films, whose Ge/(Sn + Ge) ratio varies from 0 to 1 with a step of 0.25, are shown in Fig. 3(a). The primary diffraction peaks of the as prepared CZTS/CZGS and CZTSe/CZGSe thin films match well with those of the standard diffraction peaks (JCPDS 25-0327 for CZGS, JCPDS 26-0575 for CZTS, JCPDS 52-0868 for CZTSe, and JCPDS 52-0867 for CZGSe, respectively). And three dominating peaks (112), (220)/(204) and (312)/(116) were observed in the XRD patterns of all samples. Besides, those XRD peaks of selenized sample CZTGSe are sharper and higher than that of sulfurized sample CZTGS, which indicates a better crystallinity of the former. Furthermore, with the increase of Ge/(Sn + Ge) ratio, the diffraction peaks gradually shift to higher angles due to the replacement of large Sn atom with small Ge atom. Movement of the peaks ascribed to (112) planes with defined increments of Ge is highlighted in the enlarged image in Fig. 3(b). It presents a systematic shift in the diffraction, due to the increase of Ge in an identical step (25%), as shown in the EDX analysis. It is also worth noticing that both sulfurization and selenization result in the complete alloying Ge and Sn into single-phase CZTGS and CZTGSe thin films. This is demonstrated by the fact that only a single set of peak is observed in the diffraction pattern of each thin film, rather than two distinct

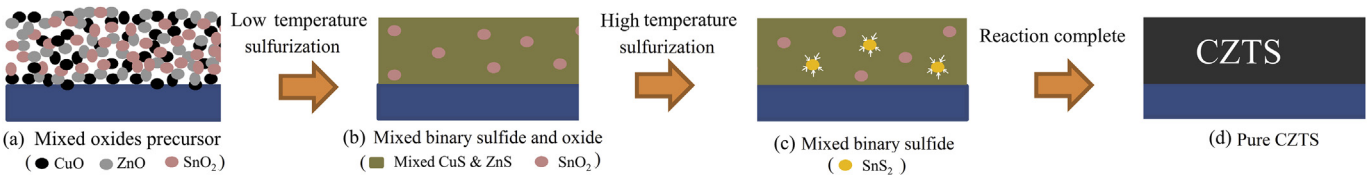

Fig. 2. The growth model of oxides nanoparticles derived CZTS thin films.

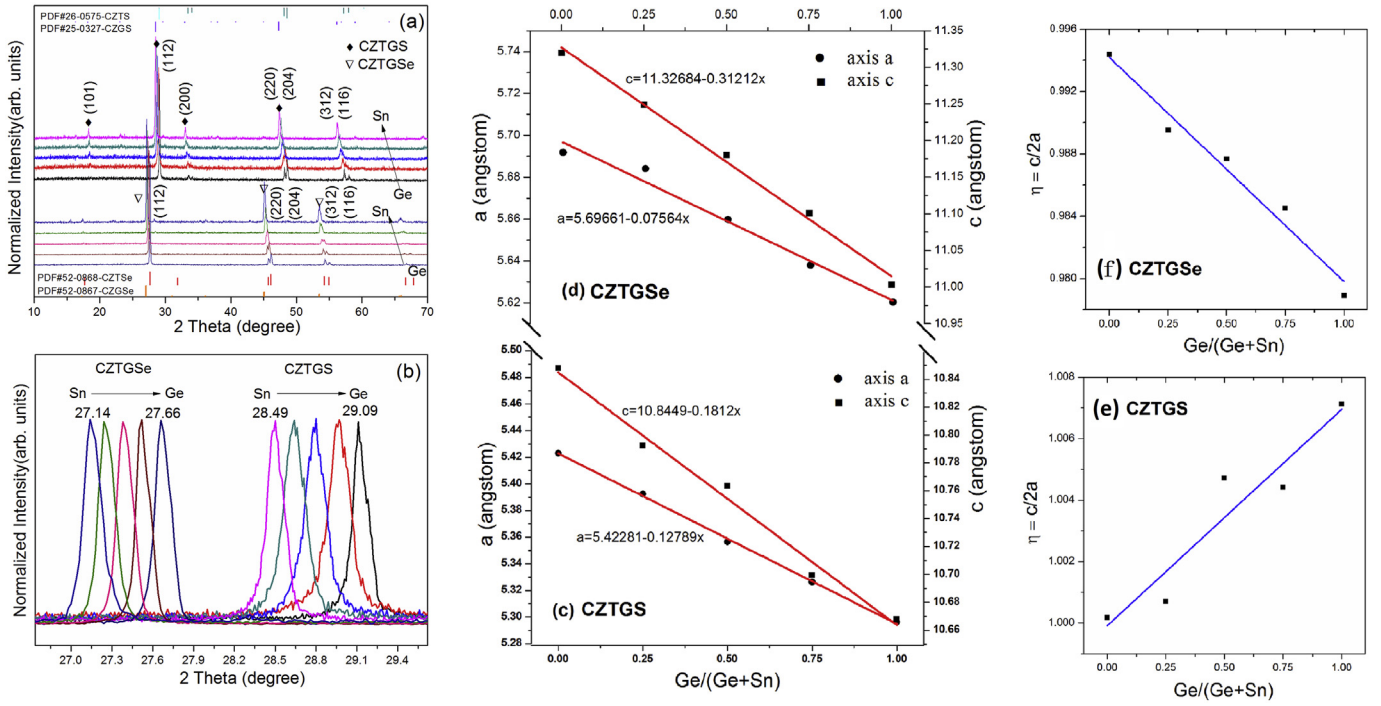

Fig. 3. The XRD patterns of (a) CZTGSe and CZTGS films, (b) the peak shift of (112) plane as the Ge content rises; Lattice parameters a and c of (c) CZTGS and (d) CZTGSe thin films; Tetragonal distortion parameter η in dependence of the Ge content in the (e) CZTGS and (f) CZTGSe thin films.

sets of peaks that would be detected if unalloyed CZTS and CZGS, CZTSe and CZGSe were present.

From the XRD patterns, the lattice constants (a and c) of the CZTGS and CZTGSe alloys as a function of Ge/(Sn + Ge) atomic ratio were calculated according to the Bragg's formula $2d\sin\theta = n\lambda$ and the approximate equation $\frac{1}{d^2} = \frac{h^2+k^2}{a^2} + \frac{l^2}{c^2}$, as shown in Fig. 3(c) and (d). For instance, the lattice constants (a and c) of CZTS and CZGS are (5.423, 10.848) Å and (5.296, 10.668) Å, while those of CZTSe and CZGSe are (5.692, 11.320) Å and (5.620, 11.003) Å. These results are all similar with the reported values of CZTS/CZGS/CZTSe/CZGSe [27–30]. As seen from Fig. 3 (c) and (d), the lattice parameter is linearly related to the Ge/(Sn + Ge) ratio, which corresponds to Vegard's law [31]. A diminution of lattice parameters of the annealed films appeared with the Ge element incorporated gradually, due to the different atom radius between Sn and Ge [29]. Meanwhile, this result also demonstrated that the substitution is feasible by using the oxides-based method, which is beneficial for the further device optimization. For another section, the tetragonal distortion parameter (η = c/2a) based on the value of Ge/(Sn + Ge) in the CZTGSe and CZTGS are shown in Fig. 3(e) and (f). It shows that when the η < 1, the CZTGSe obtained is kesterite structure (KS), while when the η > 1, the CZTGS obtained is stannite structure (ST), which agrees well with the first-principle calculations of quaternary chalcogenide semiconductors [32,33]. Both X. Zhang [34], S. Chen [35] and D. Chen [36] have revealed that η is less than 1 for the KS structure but larger than 1 for the ST structure in $Cu_2B(II)C(IV)X(VI)_4$ quaternaries, which is due to the different arrangement of Cu and Zn atoms in these two structures resulting in the different bond lengths of the Cu-VI, Zn-VI and Sn (Ge, Si)-VI bonds. L. Nieves [37] also found η is smaller than 1 for $Cu_2ZnGeTe_4$ with KS structure, which is similar to that observed in our work. However, the dependence of η on the Ge content exhibits opposite trend for CZTGS and CZTGSe. η of CZTGS increases with the increase of Ge content, whereas η of CZTGSe decreases with the increase of Ge content. Shibuya et al. [38] have also confirmed that adjusting the ratio of Fe/Zn can change the crystal structure (kesterite or stannite). Such trend is similar to the adjustment of Ge/Sn ratio in CZTGS or CZTGSe. But the mechanism for these variation of η are still unclear. Therefore, a more in-depth theoretical calculation are still needed in the further researches.

The Raman spectra of CZTGS and CZTGSe thin films are shown in Fig. 4. For Fig. 4(a), the Raman peak of the CZTS thin films which is detected at 336 cm^{-1} corresponds to what have been reported [39]. In addition, the Raman peak of the CZGS thin films at about 358 cm^{-1} is consistent with the previous result reported by Huang et al. [30]. According to the knowledge of vibration, there are 24 vibration modes in the zone center phonon of CZTS and CZGS [40]. Nevertheless only a few of them are Raman active. And the strongest one in spectrum is the A1 symmetry mode since the vibrations of S atoms are surrounded by others. Thus the Raman peaks at 336 cm^{-1} for CZTS thin films and 358 cm^{-1} for CZGS thin films are ascribed to the A1 mode [10]. Besides, Fig. 4(a), including fits with Lorentzian curves, shows double Raman peaks in CZTGS with intermediate values (i.e. x = Ge/(Sn + Ge) = 0.25, 0.5 and 0.75). This double peaks is duo to the coexistence of Ge and Sn atoms in CZTGS samples. We can see clearly from Fig. 4(a) that both A1 modes of CZTS and CZGS will shift toward the high frequency as the Ge content increases in CZTGS samples. For the selenized CZTGSe films, the strongest peak was shown at around 196 and 204 cm^{-1}, which was ascribed to the A1 mode of CZTSe and CZGSe thin film respectively. Similarly, the mixed CZTGSe thin films also indicated a shift in the Raman spectra in accordance with the changes in the Sn/Ge ratio, as shown in Fig. 4(b). However, unlike the two Raman mode in sulfurized CZTGS, the selenized CZTGSe exhibits only a symmetrical Raman peak. It may be caused by the decreased disorder of cations in the crystal lattice, compared with sulfurized CZTGS thin films. One other thing to note is that the A1 mode of CZTGS does not seem to appear in selenized CZTGSe thin films, which can be made clear by its few amount of S content. This agrees well with the EDX results. In general, the Raman peak positions of A1 mode of CZTGS and CZTGSe are all observed to move towards

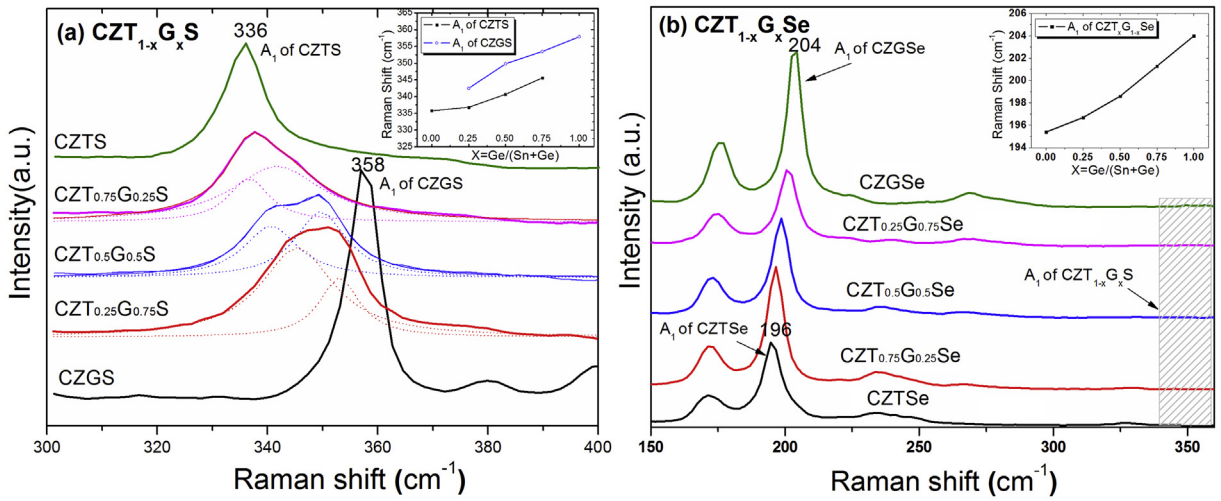

Fig. 4. Raman spectra for (a) CZTGS and (b) CZTGSe thin films. The inset is A1 Raman mode frequency dependence on Ge/(Sn + Ge) ratios.

the direction of higher frequency as the Ge ingredient rises.

Figs. 5 and 6 (a-d) show the surface and cross-sectional SEM micrographs (inset) of the CZTGS and CZTGSe thin films with different Ge content. The SEM images of all sulfurized CZTGS thin films were covered with small grains (about few hundred nanometers), as shown in Fig. 5. What's more interesting, the more Ge element in CZTGS thin films, the larger grain size will be obtained. This indicates that the Ge-alloying can boost the grain growth. However, all the CZTGS thin films are porous. After selenization, the CZTGSe thin films are more uniform, as shown in Fig. 6. Comparing with the sulfurized CZTGS thin films, the cross-sectional SEM images of the selenized CZTGSe thin films show smooth morphology and high compactness. And it seems that the Ge constituent has an effect on the size of grains, which is judged by the columnar structure and the grain size of the thin films. Chesman et al. claimed that the selenide compounds have been employed by annealing under Se atmosphere for not only tailoring the bandgap in Ge-contained sulfide phases but also triggering a vigorous densification reaction through an atomic replacement between S and Se [23]. So the selenized CZTGSe thin films with larger grain structure can be achieved in our work, compared to sulfurized CZTGS thin films. As we knows that the efficiency of polycrystalline solar cells will be improved if the compactness, grain size and homogeneity of the absorber layers are increased. So that the selenized CZTGSe thin films are superior than sulfurized ones.

To study how the structural and compositional changes stemming from alloying the thin films govern their optical properties, absorption spectroscopy measurements were conducted. Fig. 7 (a, b) shows the Tauc plots of the CZTGS and CZTGSe thin films with different germanium content. The optical energy band gap Eg of the film was determined using the relation [41]:

$$\alpha h\nu = A(h\nu - Eg)^{1/2} \quad (1)$$

where α = absorbance, h = Planck's constant and ν = frequency. The Eg were determined to be about 1.0–2.0 eV via extending the straight part of the function to make it intersect with the photon energy axis at a point, and the photon energy values of these points are similar with the values that has been reported [20]. Moreover, the Eg for both CZTGS and CZTGSe show a monotone rising with the increase of Ge content, which can be seen in Fig. 7 (c, d). The empirical relationship between the bandgap and the Ge/(Ge + Sn)

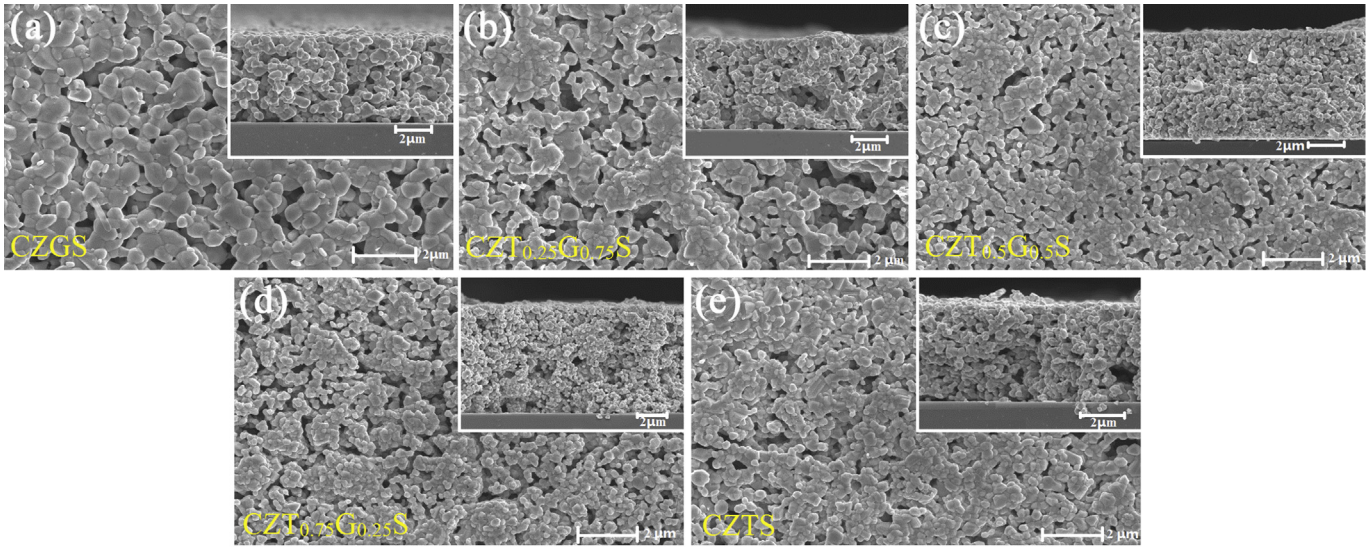

Fig. 5. The planar and cross-sectional SEM of CZTGS thin films with different Ge/(Sn + Ge) ratios.

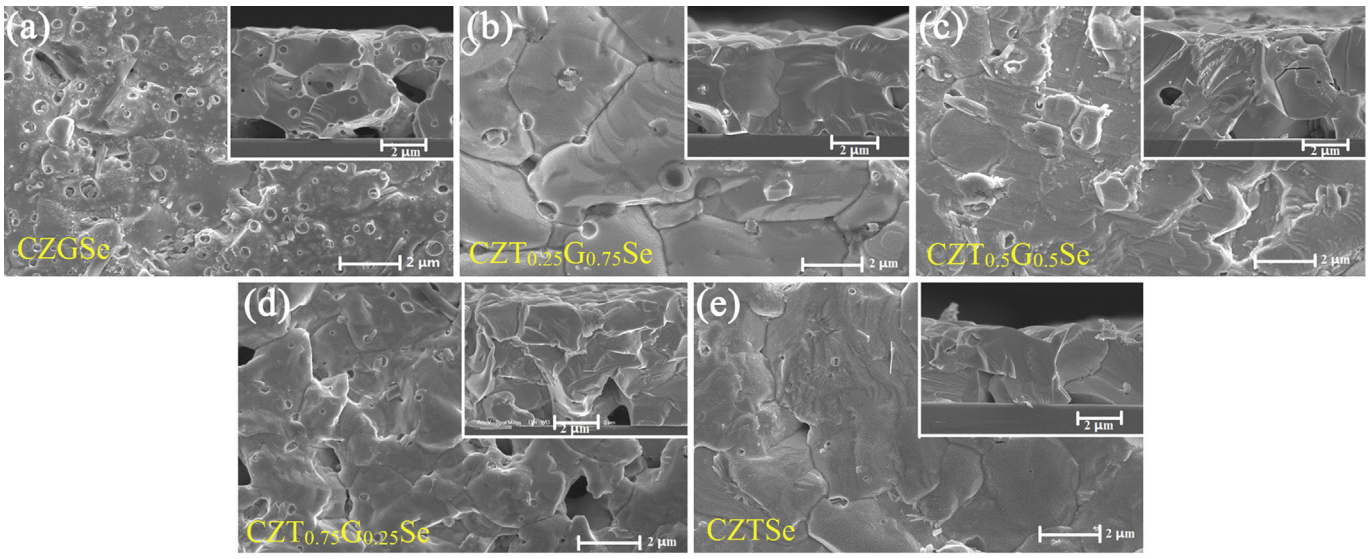

Fig. 6. The planar and cross-sectional SEM of CZTGSe thin films with different Ge/(Sn + Ge) ratios.

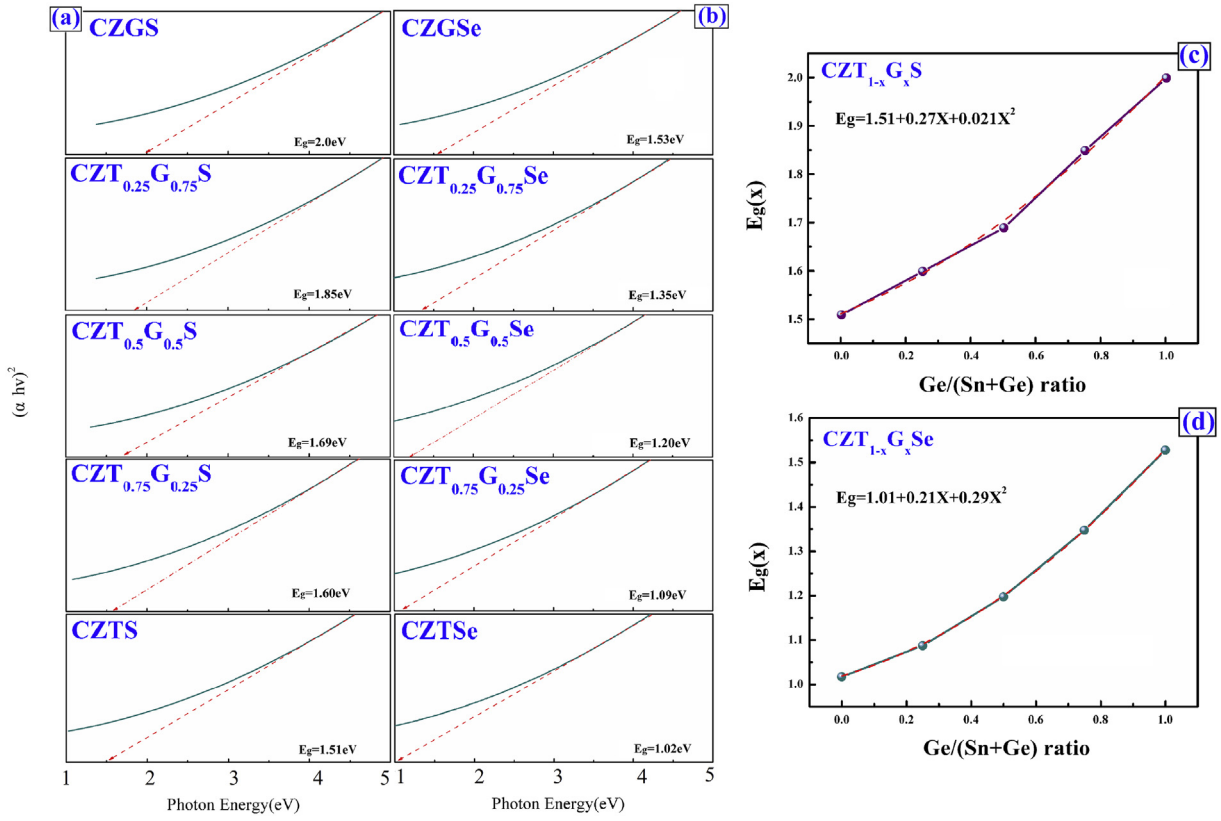

Fig. 7. Plot of $(\alpha h\nu)^2$ vs hν for the estimation of the band gap energy of CZTGS and CZTGSe thin films with different Ge/(Sn + Ge) ratios. The band-gap dependence on Ge/(Sn + Ge) ratios for (c) CZTGS and (d) CZTGSe thin films.

ratio was described by the following equation:

$$Eg\ (CZTGS\ or\ Se) = xEg\ (CZGS\ or\ Se) + (1-x)Eg\ (CZTS\ or\ Se) - bx(1-x) \quad (2)$$

where $Eg_{(CZTS\ or\ Se)}$ is 1.51 and 1.02eV, $Eg_{(CZGS\ or\ Se)}$ is 2.00 and 1.53 eV. The parameter b is so-called bowing parameter, which means the degree of nonlinearity. This parameter derived from the optical absorption data is 0.021 and 0.29eV for CZTGS and CZTGSe respectively. It indicates that CZTGSe have higher miscibility of alloyed elements than CZTGS, according to ref. [20]. On the basis of the theoretical calculations for electronic band structure, the conduction band minimum (CBM) of CZTGS or CZTGSe depends on the antibonding state of Sn-5s and Ge-4s. As replacing Sn with Ge, the

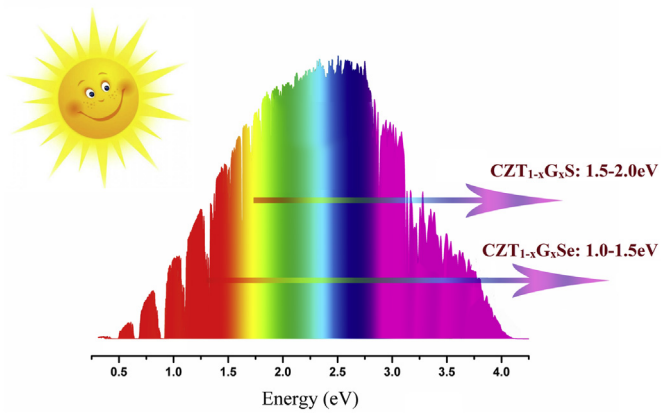

Fig. 8. Using CZTGS(e) thin films with different Sn/Ge ratios to match the solar spectrum.

repulsion of s-s and s-p orbital level between Ge and S(e) atoms are strengthened. This enhances the antibonding character of CBM, thereby increasing the bandgap [20,42]. This band gap analysis confirms that, in addition to microstructural changes, variation of the Ge/(Sn + Ge) results predictable changes of the band gap of the absorber films. The CZTGS and CZTGSe in our work are anticipated to be a promising material for the formation of full spectrum solar cells, as shown in Fig. 8. It can be seen that the absorber materials with tunable band gap in wide range can widen the light harvesting scale of the light spectrum, which is expected to achieve a further enhancement of the CZTGS(e) solar cell performance.

To investigate the effect of band-gap on the device performance, the CZTGS(e) solar cell were prepared. The Cu-poor and Zn-rich composition was used in this work, because a Zn-rich condition suppresses the substitution of Cu at Zn sites (shallow acceptors) for high efficient solar cell [43]. Fig. 9(a–c) shows the I-V curve for CZTSe, CZTS and CZGS solar cell under illumination and dark condition, respectively. The device parameters were enclosed in the figure. More information about the device characteristics have been extracted with the method introduced by Sites et al. [44], as shown in Table 2. The CZTSe, CZTS and CZGS solar cell exhibited efficiency of 3.4%, 3.08% and 0.7% without anti-reflection layer. To the best of our knowledge, this efficiency of CZTS is higher than the

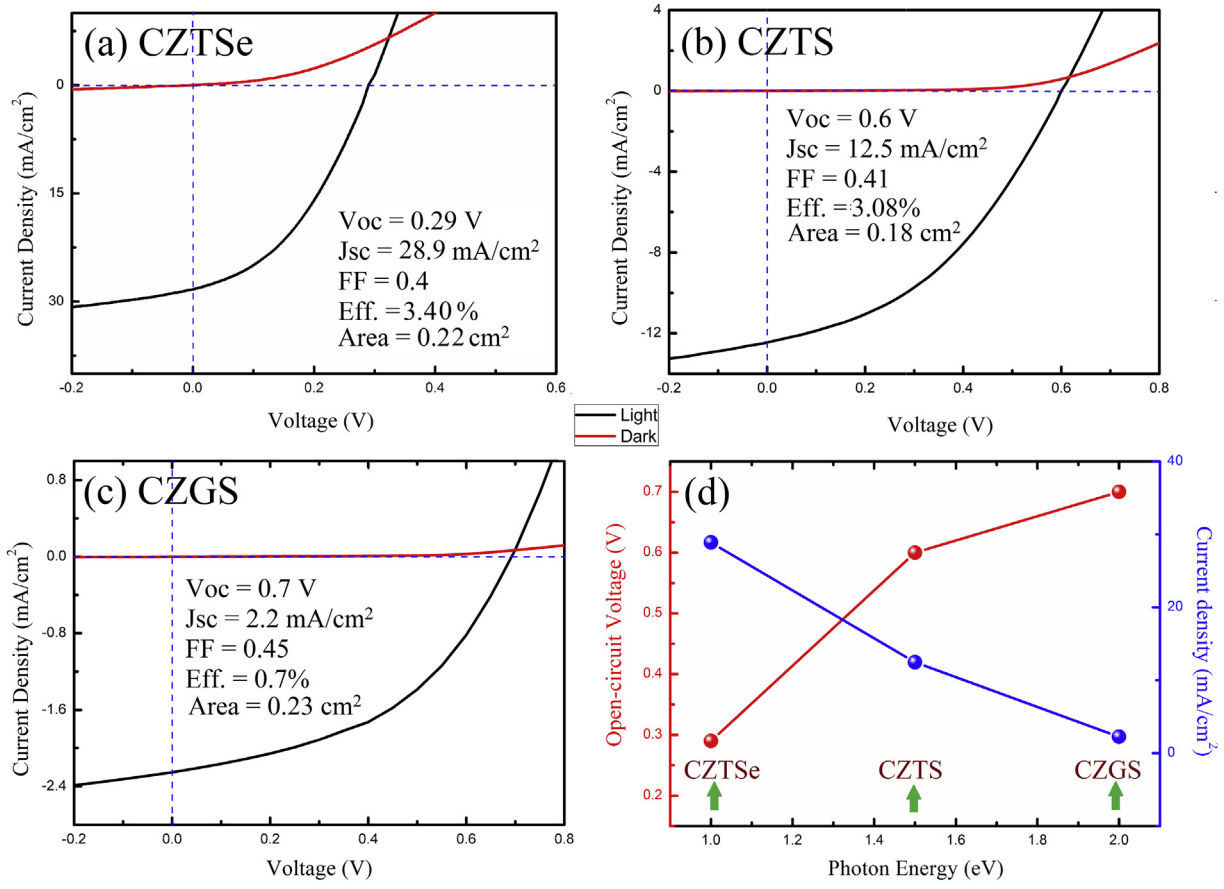

Fig. 9. J-V characteristics for (a) CZTSe, (b) CZTS and (c) CZGS solar cell under simulated AM 1.5 irradiation and dark conditions, (d) Voc and Jsc with varying band gap value.

Table 2
Device performance parameters of CZTSe, CZTS and CZGS thin film solar cells measured at room temperature.

Sample	Voc (V)	Jsc (mA/cm^2)	FF	Eff.	Area (cm^2)	Gs (mS.cm^{-2})	Rsh (Ω.cm^2)	A	J_0 (mA/cm^2)
CZTSe	0.29	28.9	0.40	3.40%	0.22	19.16	2.5	1.8	1.2×10^{-4}
CZTS	0.60	12.6	0.41	3.08%	0.18	5.73	15.5	2.1	4.0×10^{-4}
CZGS	0.70	2.2	0.45	0.70%	0.23	0.75	51.4	2.8	1.4×10^{-4}

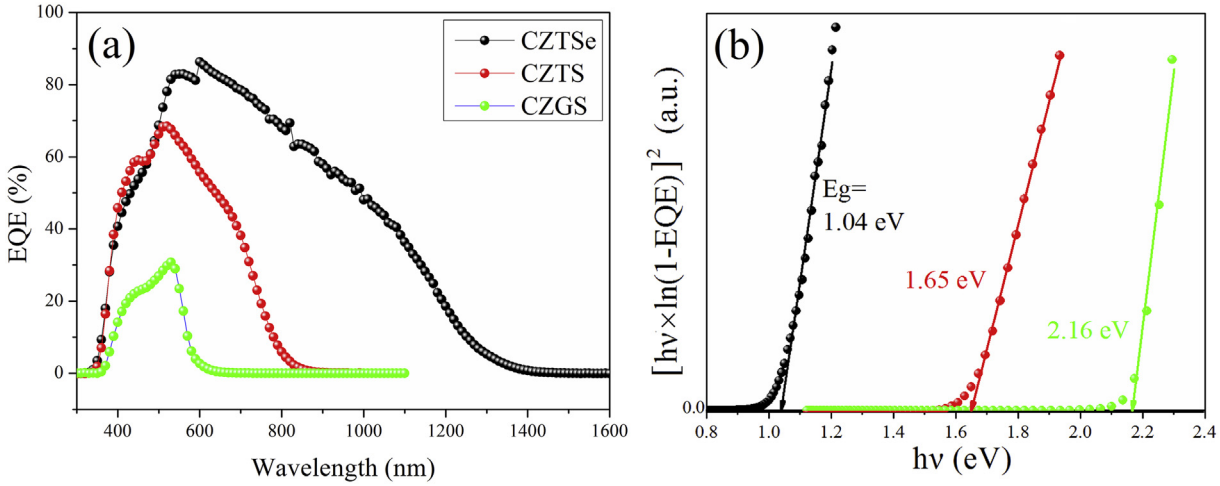

Fig. 10. (a) Quantum efficiency curve of the cell, (b) band gap determination of the cell from the EQE data.

previously-reported cells based on oxide nanoparticles derived CZTS devices [27,45]. Meanwhile, the oxide nanoparticles based CZTSe and CZGS solar cells are rarely studied. So the oxide nanoparticles-processed method is proven to be a potential route for kesterite solar cell. However, those efficiency are still lower than that of current CZTSSe champion devices [2], due to the high the shunt conductance (Gsh), series resistance (Rs), as well as ideality factor (n) (see Table 2). All the devices exhibit cross-over features, indicating a high the shunt conductance and non-ideal p-n junction properties again. It is noticed that the higher Rs of device may be attributed partly to Al:ZnO (AZO) and $MoS(e)_2$. First, the square resistance of AZO in our devices is as high as 50 Ω/□, which enlarges Rs of device. Secondly, the thick $MoS(e)_2$, caused by the high vapor pressure of S or Se, also deteriorates the performance of photovoltaic devices. While, the low Voc is attributed to the large recombination loss behaving. It may be caused by some pin holes in the films during coating process, which leaded to a current leakage path. So the optimization of device fabrication process, such as reducing Rs of AZO and thickness of $MoS(e)_2$ by introducing TiN barrier layer, is expected to improve device performance in the future work. On the other hand, the optical and electrical properties of the devices depend strongly on the bandgap value. Fig. 9(d) shows the bandgap dependence of open circuit voltage (Voc) and short circuit current density (Jsc). As the bandgap of the absorber film increases, Voc increases from 0.29 to 0.7 V, and Jsc drops from 28.9 to 2.2 mA/cm^2, which show the approximately proportional relation between Jsc/Voc and Eg. This increase of Voc is caused by larger band gap. But the Voc deficit (Eg/q - Voc) also increases with increasing Ge contents, which may be due to the increase of Fermi level pinning, band tails and bulk defects [46]. While the Jsc shows decrease because of the insufficient light absorption. The above analysis provides the foundation for increasing Voc and Jsc simultaneously by adopting multi-junction solar cells or graded-bandgap solar cells.

The external quantum efficiency (EQE) analysis of CZTSe, CZTS and CZGS thin film solar cells are shown in Fig. 10(a), which are used to confirm the influence of bandgap on carrier collection. It is seen that the EQE curves in the wavelengths from 300 to 550 nm (blue collection) exhibit a remarkable losses, due to buffer layer absorption (CdS: 530 nm) and window layers (i-ZnO/AZO: 380 nm). For wavelengths higher than 550 nm (red collection), different absorber materials (CZTSe, CZTS and CZGS) have various cut-off absorption edge as well as band gap. The bandgap of the absorber layer was extracted from the EQE curve. Fig. 10(b) plots $[h\nu \times \ln(1\text{-EQE})]^2$ against hν, where hν is incident photon energy. By using linear extrapolation, the bandgap of CZTSe, CZTS and CZGS were determined to be 1.04 eV, 1.65 eV and 2.16 eV respectively, both of which are close to the value obtained from the above absorption spectroscopy analysis. As band gap decreases, a broader absorption (longer cut-off wavelength) will be observed, allowing more photons to be absorbed. Consequently, the Jsc is enlarged, as shown in Table 3. The Jsc integrated from EQE data are about 29.6 mA/cm^2, 12.5 mA/cm^2 and 2.5 mA/cm^2 for CZTSe, CZTS and CZGS devices, which agree well with the Jsc from J-V curve. It can also see that Jsc decreases strongly (29.6 → 2.5 mA/cm^2) with the increase of the band gap (1.04 → 2.16 eV). To check the current density deficit for various devices, the max Jsc was calculated from AM1.5 solar spectrum. Given that all the photons with energy greater than the band gap are absorbed, the max Jsc of CZTSe, CZTS and CZGS devices are about 45.5 mA/cm^2, 23.8 mA/cm^2 and 11.1 mA/cm^2 respectively. So the degree of Jsc deficit expressed as (Jmax-Jsc)/Jmax (Table 3) were obtained to be 35.0%, 47.5% and 77.1% for CZTSe, CZTS and CZGS devices respectively. Once the absorber material with wider band gap was used, the larger degree of Jsc deficit was obtained. It may be due to the lower carrier mobility and lifetime of absorber material with wider band gap [47]. In addition, the non-ideal band alignment (CZTGS(e)/CdS) for devices with increasing band gap should also be taken into account. This can be confirmed by the lower EQE response (400–600 nm) for the device with wider bandgap, due to the more interfacial recombination in the device [47]. Therefore, the absorber material with small band gap is vital to the improvement of carrier collection efficiency, which provides an important guiding for fabricating high efficient device.

Table 3
Jsc integrated from EQE and max Jsc calculated from solar spectrum.

Samples	Integrated Jsc (mA/cm^2)	Max Jsc (mA/cm^2)	$\frac{(Jmax-Jsc)}{Jmax}$ (%)
CZTSe	29.6	45.5	35.0
CZTS	12.5	23.8	47.5
CZGS	2.5	11.1	77.1

4. Conclusion

In this work, a method of incorporating Ge into CZTS(e) to

obtain the CZTGS(e) solid-solution by oxide-based routes have been proposed to adjust the bandgap and lattice constants of CZTGS(e). EDX, XRD and Raman spectra are all demonstrated that the Sn and Ge atom can be highly mixed in the CZTGS(e) thin films. The lattice constants a and c of CZTGS(e) are liner with Ge content. The Raman spectrums revealed that the peak of A1 mode will move towards the direction of higher frequency when the Sn is gradually substituted by Ge, and this can be attributed to different bond-stretching force constant. According to the absorption spectra, it can be known that the band gaps of CZTGS(e) thin films can be adjusted between 1.07 and 2.00 eV by careful control of the Ge/(Sn + Ge) ratio. Finally, influence of band gap on the performance of CZTGS(e) solar cell have also been discussed detailedly. This work establishes the prospect of improvements in device efficiency through layering or adjusting the Ge ingredient, which is similar to the Ga ingredient in CIGSe.

Acknowledgment

All the work of this paper was finished under the support from National Natural Science Foundation of China (Grant No. 51502037), Natural Science Foundation of Fujian Province, China (Grant No.2015J05096) and National Key Project for Basic Research of China under (Grant No. 2011CBA00200).

References

[1] M. Kemell, M. Ritala, M. Leskela, Thin film deposition methods for $CuInSe_2$ solar cells, Crit. Rev. Solid State 30 (2005) 1–31.
[2] W. Wang, M.T. Winkler, O. Gunawan, T. Gokmen, T.K. Todorov, Y. Zhu, D.B. Mitzi, Device characteristics of CZTSSe thin-film solar cells with 12.6% efficiency, Adv. Energy Mater 4 (2014) 1301465.
[3] P. Jackson, R. Wuerz, D. Hariskos, E. Lotter, W. Witte, M. Powalla, Effects of heavy alkali elements in $Cu(In,Ga)Se_2$ solar cells with efficiencies up to 22.6%, Phys. Status Solidi RRL 10 (2016) 583–586.
[4] W. Schockley, H.J. Queisser, Detailed balance limit of efficiency of pn junction solar cells, J. Appl. Phys. 32 (1961) 510–519.
[5] S.J. Park, H.S. Jeon, J.W. Cho, Y.J. Hwang, K.S. Park, H.S. Shim, J.K. Song, Y. Cho, D.W. Kim, J. Kim, B.K. Min, Chalcogenization-derived band gap grading in solution-processed $CuIn_xGa_{1-x}(Se,S)_2$ thin-film solar cells, ACS Appl. Mater. Interfaces 7 (2015) 27391–27396.
[6] R. Caballero, C.A. Kaufmann, V. Efimova, T. Rissom, V. Hoffmann, H.W. Schock, Investigation of $Cu(In,Ga)Se_2$ thin-film formation during the multi-stage co-evaporation, Prog. Photovolt. Res. Appl. 21 (2013) 30–46.
[7] F. Liu, F. Zeng, N. Song, L. Jiang, Z. Han, Z. Su, C. Yan, X. Wen, X. Hao, Y. Liu, Kesterite $Cu_2ZnSn(S,Se)_4$ solar cells with beyond 8% efficiency by a Sol–Gel and selenization process, ACS Appl. Mater. Interfaces 7 (2015) 14376–14383.
[8] T. Rath, W. Haas, A. Pein, R. Saf, E. Maier, B. Kunert, F. Hofer, R. Resel, G. Trimmel, Synthesis and characterization of copper zinc tin chalcogenide nanoparticles: influence of reactants on the chemical composition, Sol. Energy Mater. Sol. Cells 101 (2012) 87–94.
[9] H. Wei, Z.C. Ye, M. Li, Y.J. Su, Z. Yang, Y.F. Zhang, Tunable band gap $Cu_2ZnSnS_{4x}Se_{4(1-x)}$ nanocrystals: experimental and first-principles calculations, CrystEngComm 13 (2011) 2222–2226.
[10] B.D. Khadka, J.H. Kim, Study of structural and optical properties of kesterite Cu_2ZnGeX_4 (X = S, Se) thin films synthesized by chemical spray pyrolysis, CrystEngComm 15 (2013) 10500–10509.
[11] S. Bag, O. Gunawan, T. Gokmen, Y. Zhu, D.B. Mitzi, Hydrazine-processed Ge-Substituted CZTSe solar cells, Chem. Mater. 24 (2012) 4588–4593.
[12] I. Kim, K. Kim, Y.J. Oh, K. Woo, G.Z. Cao, S. Jeong, J. Moon, Bandgap-graded $Cu_2Zn(Sn_{1-x}Ge_x)S_4$ thin-film solar cells derived from metal chalcogenide complex ligand capped nanocrystals, Chem. Mater. 26 (2014) 3957–3965.
[13] Y.W. Li, W.D. Ling, Q.F. Han, W.Z. Shi, Colloidal $Cu_2Zn(Sn_{1-x}Gex)S_4$ nanocrystals: electrical properties and comparison between their wurtzite and kesterite structures, RSC Adv. 4 (2014) 55016–55022.
[14] K. Biswas, S. Lany, A. Zunger, The electronic consequences of multivalent elements in inorganic solar absorbers: multivalency of Sn in Cu_2ZnSnS_4, Appl. Phys. Lett. 96 (2010) 201902.
[15] G.M. Ford, Q.J. Guo, R. Agrawal, H.W. Hillhouse, Earth abundant element $Cu_2Zn(Sn_{1-x}Ge_x)S_4$ nanocrystals for tunable band gap solar cells: 6.8% efficient device fabrication, Chem. Mater. 23 (2011) 2626–2629.
[16] M. Grossberg, K. Timmo, T. Raadik, E. Kärber, V. Mikli, J. Krustok, Study of structural and optoelectronic properties of $Cu_2Zn(Sn_{1-x}Ge_x)Se_4$ (x=0 to 1) alloy compounds, Thin Solid Films 582 (2015) 176–179.
[17] S. Kim, K.M. Kim, H. Tampo, H. Shibata, K. Matsubara, S. Niki, Ge-incorporated $Cu_2ZnSnSe_4$ thin-film solar cells with efficiency greater than 10%, Sol. Energy Mater. Sol. Cells 144 (2016) 488–492.
[18] M. Neuschitzer, J. Marquez, S. Giraldo, M. Dimitrievska, M. Placidi, I. Forbes, V. Izquierdo-Roca, A. Pérez-Rodriguez, E. Saucedo, Voc boosting and grain growth enhancing ge-doping strategy for $Cu_2ZnSnSe_4$ photovoltaic absorbers, J. Phys. Chem. C 120 (2016) 9661–9670.
[19] D.B. Khadka, S. Kim, J. Kim, Effects of Ge alloying on device characteristics of kesterite-based CZTSSe thin film solar cells, J. Phys. Chem. C 120 (2016) 4251–4258.
[20] D.B. Khadka, J.H. Kim, Band gap engineering of alloyed $Cu_2ZnGe_xSn_{1-x}$ Q_4 (Q= S, Se) films for solar cell, J. Phys. Chem. C 119 (2015) 1706–1713.
[21] L. Shi, P.G. Yin, Phosphate-free synthesis, optical absorption and photoelectric properties of Cu_2ZnGeS_4 and $Cu_2ZnGeSe_4$ uniform nanocrystals, Dalton Trans. 42 (2013) 13607–13611.
[22] L. Shi, P.G. Yin, H.J. Zhu, Q. Li, Synthesis and photoelectric properties of Cu_2ZnGeS_4 and $Cu_2ZnGeSe_4$ single-crystalline nanowire arrays, Langmuir 29 (2013) 8713–8717.
[23] A.S.R. Chesman, V.E. Joel, D.G. Enrico, N.W. Duffy, N.A.S. Webster, J.J. Jasieniak, Cu_2ZnGeS_4 nanocrystals from air-stable precursors for sintered thin film alloys, Chem. Mater. 26 (2014) 5482–5491.
[24] J. He, L. Sun, Y. Chen, J. Jiang, P. Yang, J. Chu, Influence of sulfurization pressure on Cu_2ZnSnS_4 thin films and solar cells prepared by sulfurization of metallic precursors, J. Power Sources 273 (2015) 600–607.
[25] R.E. Nikolaev, I.G. Vasilyeva, A new way of phase identification of $AgGaGeS_4 \cdot nGeS_2$ crystals, J. Solid State Chem. 203 (2013) 340–344.
[26] G. Chen, C. Yuan, J. Liu, Z. Huang, S. Chen, W. Liu, G. Jiang, C. Zhu, Fabrication of Cu_2ZnSnS_4 thin films using oxides nanoparticles ink for solar cell, J. Power Sources 276 (2015) 145–152.
[27] L.J. Chen, Y.J. Chuang, Directly electrospinning growth of single crystal Cu_2ZnSnS_4 nanowires film for high performance thin film solar cell, J. Power Sources 241 (2013) 259–265.
[28] J. Bi, L. Yao, J. Ao, S. Gao, G. Sun, Q. He, Z. Zhou, Y. Sun, Y. Zhang, Pulse electrodeposition of copper on molybdenum for $Cu(In,Ga)Se_2$ and $Cu_2ZnSnSe_4$ solar cell applications, J. Power Sources 326 (2016) 211–219.
[29] S. Nakamura, T. Maeda, T. Wada, Phase stability and electronic structure of In-free photovoltaic materials: $Cu_2ZnSiSe_4$, $Cu_2ZnGeSe_4$, and $Cu_2ZnSnSe_4$, Jpn. J. Appl. Phys. 49 (2010) 121203.
[30] L. Huang, H.M. Deng, J. He, X.K. Meng, L. Sun, P.X. Yang, J.H. Chu, Synthesis of Cu_2ZnGeS_4 thin film via sulfurization of RF magnetron sputtered precursor, J. Mater. Sci. Mater. Electron 26 (2015) 3984–3988.
[31] L. Vegard, Die konstitution der mischkristalle und die raumfüllung der atome, Z. Phys. 5 (1921) 17.
[32] Y.B. Zhang, X.D. Sun, P.H. Zhang, X. Yuan, F.Q. Huang, W.Q. Zhang, Structural properties and quasiparticle band structures of Cu-based quaternary semiconductors for photovoltaic applications, J. Appl. Phys. 111 (2012) 0637091–0637096.
[33] O.V. Parasyuk, L.V. Piskach, Y.E. Romanyuk, I.D. Olekseyuk, V.I. Zaremba, V.I. Pekhnyo, Phase relations in the quasi-binary Cu_2GeS_3-ZnS and quasi-ternary Cu_2S-Zn(Cd)S-GeS_2 systems and crystal structure of Cu_2ZnGeS_4, J. Alloys Compd. 397 (2005) 85–94.
[34] X. Zhang, D. Rao, R. Lu, K. Deng, D. Chen, First-principles study on electronic and optical properties of $Cu_2ZnSiVI_4$ (VI=S, Se, and Te) quaternary semiconductors, AIP Adv. 5 (2015) 057111.
[35] S.Y. Chen, X.G. Gong, A. Walsh, S.H. Wei, Electronic structure and stability of quaternary chalcogenide semiconductors derived from cation cross-substitution of II-VI and I-III-VI_2 compounds, Phys. Rev. B 79 (2009) 165211.
[36] D. Chen, N.M. Ravindra, Electronic and optical properties of Cu_2ZnGeX_4 (X=S, Se and Te) quaternary semiconductors, J. Alloys Compd. 579 (2013) 468–472.
[37] L. Nieves, G.E. Delgado, G. Marcano, Ch. Power, S.A. Lopez-Rivera, C. Rincon, Structural characterization of the high-temperature modification of the $Cu_2ZnGeTe_4$ quaternary semiconductor compound, Phys. Status Solidi B 253 (2016) 1195–1201.
[38] T. Shibuya, Y. Goto, Y. Kamihara, M. Matoba, K. Yasuoka, L.A. Burton, A. Walsh, From kesterite to stannite photovoltaics: stability and band gaps of the $Cu_2(Zn, Fe)SnS_4$ alloy, Appl. Phys. Lett. 104 (2014) 021912.
[39] P.A. Fernandes, P.M.P. Salomé, A.F. da Cunha, Growth and Raman scattering characterization of Cu_2ZnSnS_4 thin films, Thin Solid Films 517 (2009) 2519–2523.
[40] J. Chen, W. Li, C. Yan, S.J. Huang, X.J. Hao, Studies of compositional dependent $Cu_2Zn(Ge_xSn_{1-x})S_4$ thin films prepared by sulfurizing sputtered metallic precursors, J. Alloy Compd. 621 (2015) 154–161.
[41] N. Revathi, P. Prathap, R.W. Miles, K.T. Ramakrishna Reddy, Annealing effect on the physical properties of evaporated In_2S_3 films, Sol. Energy Mater. Sol. Cells 94 (2010) 1487–1491.
[42] Q. Shu, J.H. Yang, S. Chen, B. Huang, H. Xiang, X.G. Gong, S.H. Wei, $Cu_2Zn(Sn,Ge)Se_4$ and $Cu_2Zn(Sn,Si)Se_4$ alloys as photovoltaic materials: structural and electronic properties, Phys. Rev. B 87 (2013) 1152081–1152085.
[43] S. Chen, X.G. Gong, A. Walsh, S. Wei, Defect physics of the kesterite thin-film solar cell absorber Cu_2ZnSnS_4, Appl. Phys. Lett. 96 (2010) 021902.
[44] J.R. Sites, P.H. Hauk, Diode quality factor determination for thin-film solar cells, Sol. Cells 27 (1989) 411–417.
[45] X. Jin, J. Li, G. Chen, C. Xue, W. Liu, C. Zhu, Preparation of Cu_2ZnSnS_4-based thin film solar cells by a combustion method, Sol. Energy Mat. Sol. Cells 146 (2016) 16–24.

[46] H. Xie, M. Dimitrievska, X. Fontané, Y. Sánchez, S. López-Marino, Izquierdo-Roca, V. Bermúdez, A. Pérez-Rodrígue, E. Saucedo, Formation and impact of secondary phases in Cu-poor Zn-rich $Cu_2ZnSn(S_{1-y}Se_y)_4$ ($0 \leq y \leq 1$) based solar cells, Sol. Energy Mater. Sol. Cells 140 (2015) 289–298.

[47] J. Li, H. Wang, M. Luo, J. Tang, C. Chen, W. Liu, F. Liu, Y. Sun, J. Han, Y. Zhang, 10% Efficiency $Cu_2ZnSn(S,Se)_4$ thin film solar cells fabricated by magnetron sputtering with enlarged depletion region width, Sol. Energy Mat. Sol. Cells 149 (2016) 242–249.